Final Report

Project Title:	Recovery Act: "Near-Single-Crystalline Photovoltaic Thin Films on Polycrystalline, Flexible Substrates"
Covering Period:	Aug. 1, 2009 to July 30, 2010
Date of Report:	October 22, 2010
Recipient:	University of Houston
Award Number:	DE-EE0000578
Working Partners:	None
Cost-Sharing Partners:	None

Contacts:

Dr. Venkat Selvamanickam
Phone: 713-743-4044
Fax: 713-743-4513
Email: selva@uh.edu

Vanessa Stepney
Phone: 713-743-9205
Email: vstepney@uh.edu

DOE Project Team:	DOE Field Contracting Officer	- Andrea Lucero
	DOE Field Project Officer	- Brian Hunter
	Project Engineer	-

Project Objective: The objective of the project is to evaluate a novel concept for doubling the efficiency of thin film photovoltaics (PV) while benefiting from the advantage of thin film manufacturing by the use of less material and roll-to-roll continuous processing. The goal of the project is to achieve efficiency levels obtained so far only with single crystalline wafer-based PV using a novel approach to create near-single-crystalline PV thin films on inexpensive polycrystalline flexible substrates.

Background: Photovoltaic cells with efficiencies at the higher end of the spectrum are expensive due to high materials costs. Cells based on III-V compounds have exhibited efficiencies of about 40%, but have found only limited use because of their cost, which is primarily driven by the high cost of single crystal substrates. Additionally, multi-junction or tandem cells which have resulted in high efficiencies in both Si and III-V compounds have been viable only with single crystalline individual cells. On the other end of the spectrum, thin film solar cells offer the advantage of low-cost fabrication, but have not yielded the higher efficiencies of single crystalline cells. Hence, achievement of near-single-crystalline thin film photovoltaics on polycrystalline substrates concomitantly with a low density of defects can be game-changing in the photovoltaic research arena by combining high efficiency with low cost.

The overarching objective of this program is to demonstrate proof-of-concept of a processing technology that would enable a roll-to-roll processing of inexpensive ultra-high efficient III-V thin film photovoltaics on inexpensive, flexible polycrystalline substrates. Our process method to achieve near-single-crystalline epitaxial photovoltaic thin films on polycrystalline substrates is built on a foundation successfully demonstrated outside the PV industry for transmitting electric power. One of the enablers in the thin film multilayer architecture used in this program is a biaxially-textured template made by ion beam-assisted deposition (IBAD). When IBAD templates are directly applied to fabricate epitaxial photovoltaic films however, these crystalline defects are expected to be deleterious to their properties. Misfit dislocations at the interfaces can lead to threading dislocations propagating into the bulk of the film. Hence, in addition to the first enabler, namely biaxially-textured IBAD templates, another type of enabler is needed to grow single crystalline photovoltaic thin films with minimal defects.

An example of an architecture of multilayer structures is being synthesized and investigated in this study is shown in Figure 1.

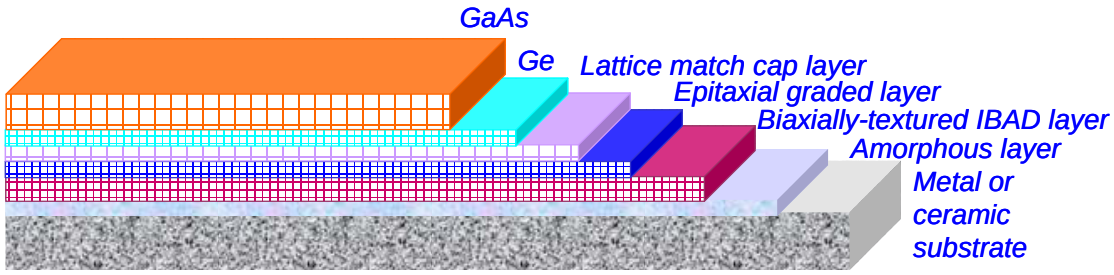

Figure 1. *Schematic of the photovoltaic cell structure based on single crystalline films on polycrystalline substrate*

Major Accomplishments in this Program:

- Single-crystalline-like Ge films with in-plane texture of about 6° were successfully grown on the buffered IBAD MgO templates on flexible, inexpensive metal substrates.
- Identification that structural match is critical to achieve epitaxial Ge and demonstration of epitaxy using fluorite CeO_2.
- Found that the in-plane texture became considerably sharp as Ge film thickness was increased. An in-plane texture as sharp as 1° FWHM was achieved in a 6 μm film indicating an average grain-to-grain misorientation as small as 1° over the entire sample.

- Cross sectional TEM conducted even in a difficult metal-oxide-semiconductor architecture. Evaluated how the defect density changed with film thickness.
- Found that several of the defects in Ge layer could have propagated even from MgO layer and through the $LaMnO_3$, CeO_2 and into the Ge layer. Found that the defect density is reduced significantly in the top part of a thick Ge film.
- Developed a procedure for defect density identification by etch pit density method and found that the results were consistent with the results obtained from High resolution XRD.
- Demonstrated single crystalline-like, anti-phase-defect-free, 1 micron-thick GaAs epilayers on Ge on IBAD templates on flexible metal substrates.
- Temperature dependent photoluminescence (PL) analysis revealed a strong PL in as-grown GaAs on metal substrates. The magnitude of red-shift (13 meV) suggested the absence of any significant thermoelastic/lattice mismatch strain (ε<0.1%) in the epilayers.
- Investigated device design strategies that would support development of high-efficiency devices in presence of dislocation densities of 10^8 cm^{-2} present in our epitaxial GaAs films. Results from modeling work show that with a proper emitter, base and doping selection, the modeled efficiency of a GaAs cells with dislocation densities of 10^9 and 10^8 cm^{-2} could be increased from 1% and 7% to 11% and 17% respectively. Under AM0, this single junction GaAs solar cell, has optimized value of emitter and base thickness of around 0.7 and 1.7 microns respectively, to give a maximum efficiency of 24.2%
- Fabricated complete GaAs solar cells using our Ge films on metal substrates. Pattern resolution of few microns with well-defined grid line of 30 microns has been realized on few cm square flexible templates.
- Two solar cells were fabricated using the architecture discussed previously. Unfortunately, they were found to be shorted. TEM analysis shows presence of Ge in the GaAs layer, presence of substrate species in the Ge layer as well as an undulating top contact layer. Any or all of these could have contributed to the short. We are working on addressing these issues and evaluate the benefit of our demonstration of epitaxial III-V solar cells on inexpensive substrates.

Details of Accomplishments:

Task 1: Fabrication of biaxially-textured MgO thin films on Hastelloy C-276 substrates by ion beam-assisted deposition (IBAD)

Highly polished Hastelloy C-276 substrates have been prepared by electropolishing. The surface roughness of the substrates was confirmed to be less than 1 nm. Amorphous alumina and nanocrystalline yttria were deposited on the substrates by magnetron sputtering. Biaxially-textured MgO films have been made on alumina-yttrria buffered Hastelloy substrates by Ion Beam Assisted Deposition (IBAD). Growth parameters of IBAD MgO such as beam voltage, beam current, acceleration voltage and ion-to-atom arrival ratio were appropriately chosen to achieve a good degree of textured as monitored by in situ Reflection High Energy Electron Diffraction (RHEED). Epitaxial buffer layers of MgO and $LaMnO_3$ have been deposited on these substrates by magnetron sputtering. In-plane texture measurements conducted on these buffer layers by X-ray Diffraction show excellent values of 6 to 7 degrees.

Task 2. Graded epitaxial buffer stack deposition on IBAD MgO for lattice match with Ge

All Ge films reported in this work were deposited using the following conditions except for deposition temperature variations. 50 nm thick Ge was grown using a reel-to-reel r.f. magnetron sputtering system using Ge targets. The deposition was conducted at 250 W at a pressure of 4 mTorr in an atmosphere of Ar-4% H_2 (4% H_2 with remainder Ar) at a tape moving speed of 2 cm/min. First, the homo-epitaxial MgO films were used as template to grow Ge films. Six samples were fabricated at deposition temperatures of 600, 650, 720, 770, 820 and 850ºC all in a single run without venting the system. Reel-to-reel systems provide this benefit of multiple deposition conditions in a single run by which unintended variations from run to run can be avoided as well as exploration of a large range of process parameters can be expedited.

Theta-2theta XRD measurements conducted on all samples showed polycrystalline Ge films with all major crystallographic orientations. Also, the desired (400) peak of Ge was found to be weak in all samples. Figure 2 exhibits a theta-2theta pattern obtained from a Ge film grown on MgO at 600ºC showing intense (220) and weaker (111), (400) and (311) Ge peaks. It was clear that epitaxial growth of Ge was not possible directly on MgO. The lattice parameter of MgO is 4.22 Å and that of Ge is 5.646 Å. The edge-on-edge lattice mismatch between the two materials is quite high – 33.8%. However, we expect, based extensive experience with heteroepitaxial growth of various materials on IBAD templates, that Ge could grow rotated by 45° within the film plane, i.e. [100] direction of Ge matching with [110] direction of MgO. In such an instance, the lattice mismatch can be substantially reduced. However, even with this rotation, there would exist a large lattice mismatch between MgO and Ge (5.4%).

Next, in order to minimize the lattice mismatch, we deposited an intermediate layer of epitaxial $LaMnO_3$ on the homo-epi MgO film. $LaMnO_3$ has been previously successfully employed as a cap layer on IBAD MgO-based templates for growth of high performance oxide superconducting films. Further, the lattice parameters in the basal plane of $LaMnO_3$ are a = 5.53 Å and b = 5.71 Å which results in lattice mismatch with Ge of -2.1% and 1.1% respectively, much better than in the case of MgO. Additionally, it was expected that edge-on-edge epitaxy of Ge, without 45° rotation should be possible. $LaMnO_3$ was deposited by r.f. sputtering about 30 - 50 nm in thickness was grown on the homoepitaxial MgO on IBAD MgO at a temperature of 700ºC to 750ºC. XRD measurements on the $LaMnO_3$ films confirmed heteroepitaxial growth with an in-plane texture of 6 to 7º FWHM.

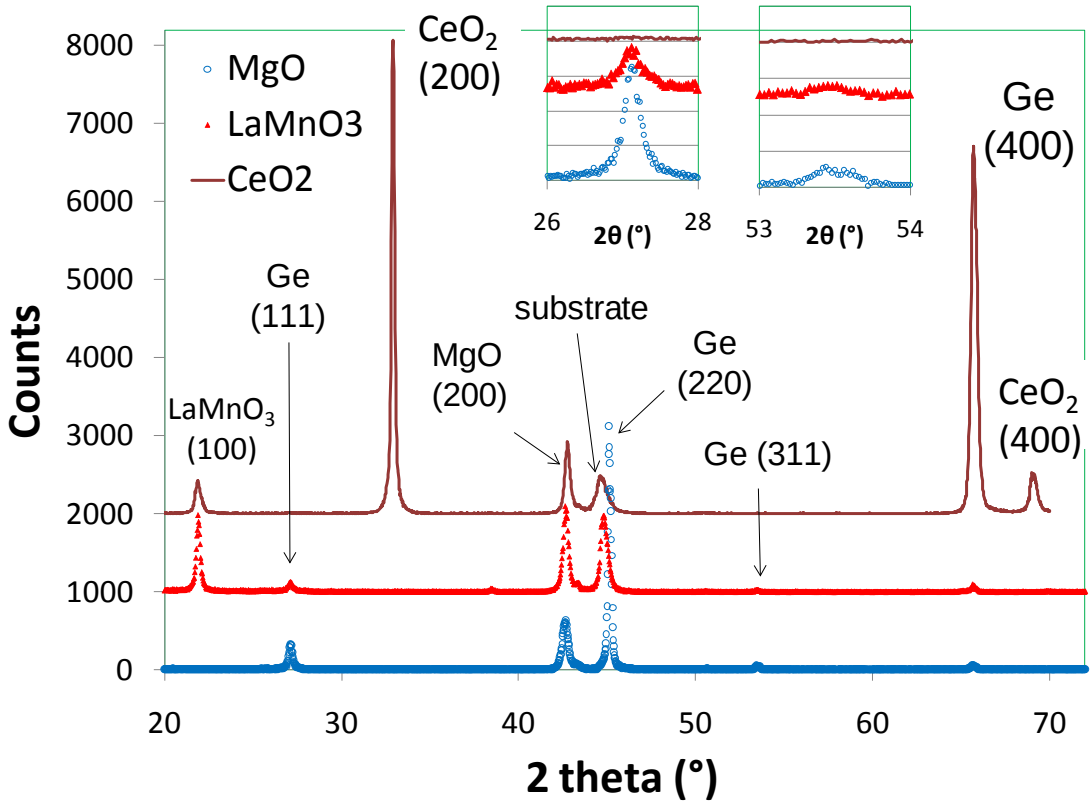

Figure 2. *Theta-2theta XRD patterns obtained from Ge film grown at 600ºC/580ºC directly on homo-epitaxial MgO, $LaMnO_3$ and on CeO_2 all atop IBAD template on flexible hastelloy substrate. The insets show data in the vicinity of Ge (111) and Ge (311) peaks.*

Ge films of identical thickness of about 50 nm were then deposited on five $LaMnO_3$ buffered IBAD tapes at deposition temperatures of 500, 530, 550, 580, and 650ºC. XRD theta-2theta pattern obtained from a Ge film deposited at 580ºC on $LaMnO_3$ on IBAD template is shown in Figure 2. This film as well those grown at other temperatures

showed signs of polycrystalline Ge growth. (111) and (311) peaks of Ge are clearly evident in addition to a weak (400) peak. The fact that even with a much improved lattice match, Ge did not grow epitaxially on $LaMnO_3$ indicated that there should be other factors key for epitaxial growth of Ge using IBAD templates such as structural and chemical incompatibilities. Chemical incompatibility could be due to formation of an intermediate phase between $LaMnO_3$ and Ge although no such information has been found in the literature. We have successfully grown non oxides such as Ni epitaxially on $LaMnO_3$ as well as on MgO using IBAD templates and it is not obvious why there would be a chemical compatibility issue in the growth of Ge on $LaMnO_3$ or on MgO.

Structural incompatibility could be due to the lack of match of the atomic locations of in the basal plane of Ge and $LaMnO_3$. Figure 3 provides details of basal plane projections of atomic locations in materials studied in this work. As seen in the figure, Ge has a diamond structure with atoms in the four tetrahedral hole locations, projections of which on the basal plane are at ¼,¼,0, ¼,¾,0, ¾,¼,0 and ¾,¾,0. $LaMnO_3$ and MgO possess a perovskite structure and rock-salt structure respectively with no atoms in the tetrahedral holes and hence do not have a good structural match with Ge.

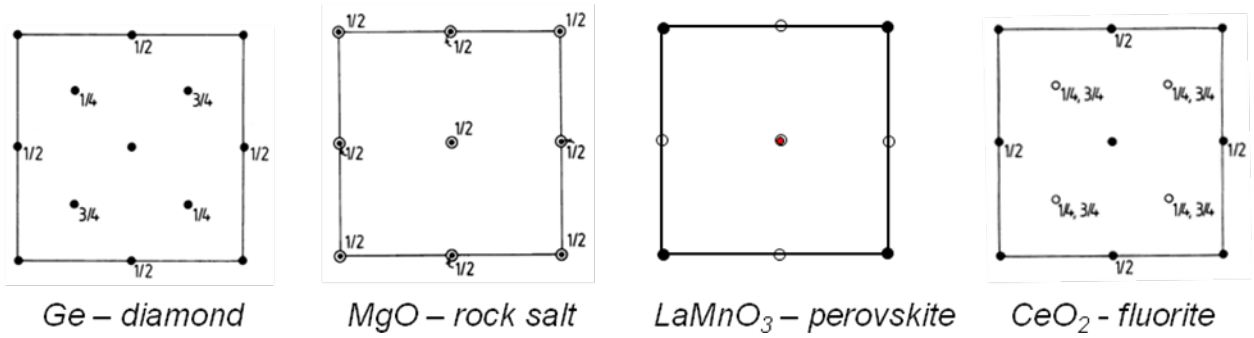

Figure 3. *Basal plane projections of atomic locations in MgO and epitaxial layers grown. The best structural match is obtained between Ge and fluorite CeO_2.*

We then focused specifically on the issue of structural compatibility between Ge and the underlying oxide layer. In this regards, we investigated an alternate layer, CeO_2, between Ge and IBAD MgO. The lattice parameter of CeO_2 is 5.41 Å which results in a high mismatch of -4.5% with Ge, almost as high as that between MgO and Ge (considering 45° rotation of Ge lattice on MgO). We still chose CeO_2 because of its better structural match with Ge. As shown in Figure 3, CeO_2 has a fluorite structure with atoms in the eight tetrahedral hole locations, projections of which on the basal plane are at ¼,¼,0, ¼,¾,0, ¾,¼,0 and ¾,¾,0 which match perfectly with the atomic locations of Ge. A meter-long CeO_2 film was deposited on $LaMnO_3$ on homoepitaxial MgO on IBAD template in the same reel-to-reel magnetron sputtering system using conditions of 300

W, 820ºC, 4 mTorr, in an atmosphere of Ar-O_2 and at a tape speed of 1.4 cm/min. XRD measurements confirmed epitaxial growth of CeO_2.

Ge films were then deposited on six CeO_2 buffered IBAD tapes at deposition temperatures of 500, 550, 580, 600, 640, 670 and 720ºC. XRD theta-2theta pattern obtained from a Ge film deposited at 600ºC on CeO_2 on IBAD template is shown in Figure 2. The presence of an intense single orientation of CeO_2 (200) is obvious in the figure. Also, a strong Ge (400) orientation is seen, much stronger than the (400) peaks observed in Ge films grown directly on MgO and $LaMnO_3$. No evidence of (111) or other peaks of Ge is present indicating the preferential out-of-plane texture of (400) in the Ge film. The insets in Figure 2 show the clear absence of (111) and (311) peaks of Ge compared with the films grown on MgO and $LaMnO_3$.

Figure 4 displays theta-2theta XRD patterns obtained from Ge films deposited over a temperature range of 500 to 720ºC focusing in the angular range of the Ge (400) peak. It is seen from the figure that the most intense Ge (400) peak occurs in the samples deposited at 580ºC and 600ºC. The Ge (400) peak intensity is diminished at lower and higher deposition temperatures. Interestingly, even though the same CeO_2 film was used for growth of all six samples of Ge, it seen from Figure 2 that the CeO_2 (400) peak intensity itself becomes weaker at higher temperatures. It is possible that the ceria layer is modified by the reducing atmosphere using in the deposition of Ge at higher deposition temperatures. If that is the case, then a proper template will not be available for epitaxial Ge growth which could explain the weaker Ge peaks at higher deposition temperatures.

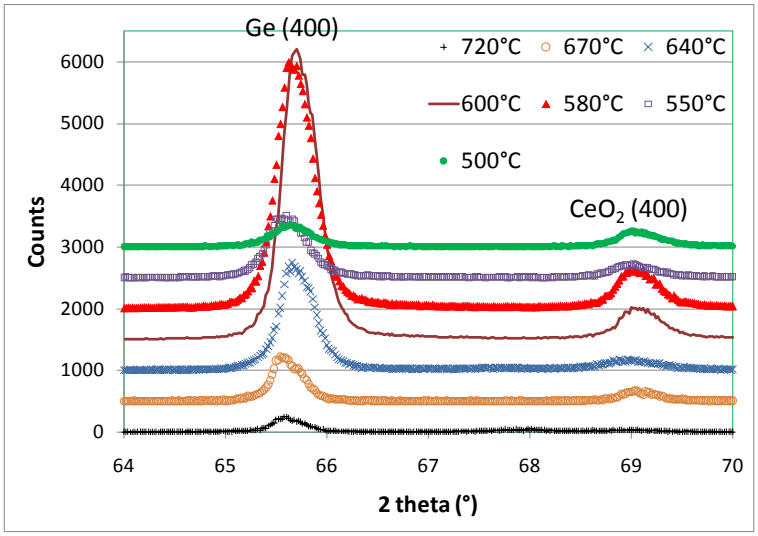

Figure 4. *Ge (400) and CeO_2 (400) peak intensities in Ge films grown at a temperature range of 500ºC - 720ºC on CeO_2 overlying IBAD template.*

The in-plane texture of Ge was measured by XRD (111) polefigure measurements of Ge and the data is shown in Figure 5. A clear four-fold symmetry is shown in the figure without the presence of other orientations. This result clearly demonstrates strong biaxial texture achieved in Ge epitaxially grown on CeO_2 on IBAD MgO template on metal substrate. The spread in the in-plane texture of Ge is calculated to be 6.6º FWHM which is comparable to that of the underlying IBAD MgO template. Based on our work on superconducting oxide films on IBAD templates, we expect that this texture can be sharpened with growth of thicker heteroepitaxial layers.

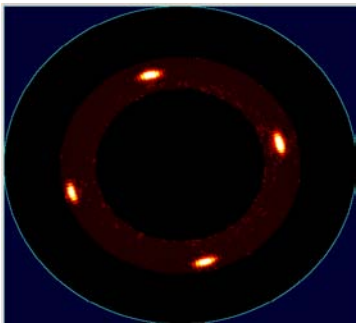

Figure 5. *(111) polefigure of Ge film deposited at 600ºC on CeO_2 overlying IBAD template.*

High-resolution X-ray Diffraction data was obtained from the (004) peak of Ge film and the data is shown in Figure 6. The peak is found to be sharp at 2800 arcsec indicating the strong texture and crystallinity of the film. The width of the peak indicates a defect density in the range of 10^8 to 10^9 cm^{-2} which needs to be improved for device quality III-V semiconductor growth.

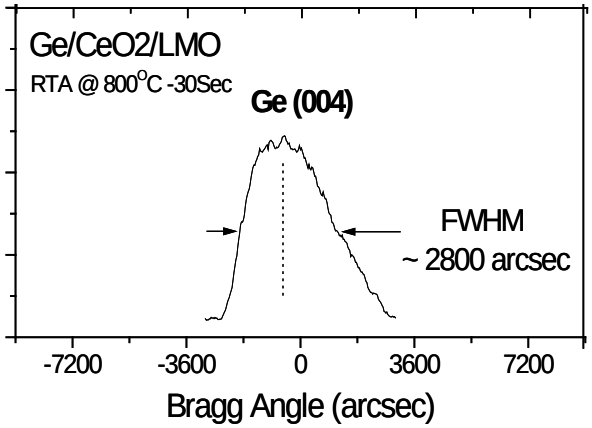

Figure 6. *High resolution X-ray Diffraction scan obtained from (004) peak of Ge grown on CeO_2 overlying IBAD template.*

Surface roughness and topography examination of the Ge films grown at various temperatures on CeO_2 on IBAD template was conducted using atomic force microscopy (AFM) and scanning electron microscopy (SEM). Results from a Ge film deposited at 600°C are shown in Figure 7. The RMS surface roughness of the film is found to be about 9 nm which is similar to that measured on Ge grown at lower temperatures. But, this value is significantly higher than the surface roughness of 2 to 3 nm measured in the CeO_2 layer. Further, the surface roughness was found to increase to about 17 nm in Ge films grown at higher temperatures. So, 600°C is an optimum deposition temperature from the viewpoint of sharpness of texture and film smoothness. As seen in Figure 6, the grain size of Ge film grown at 600°C is about 200 nm. This value is comparable to the grain size of the IBAD MgO film deposited at room temperature and indicates that no significant grain growth occurred in subsequent deposition of epitaxial layers at high temperature.

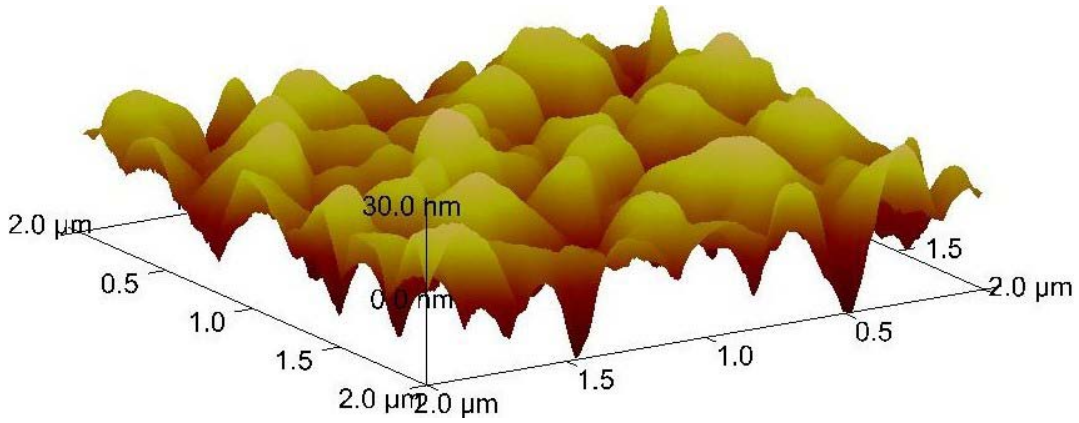

(a)

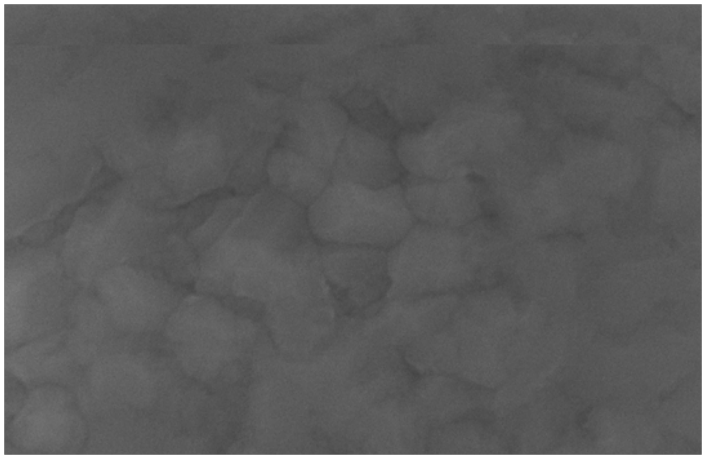

(b)

Figure 7. *AFM (a) and SEM (b) images obtained from Ge film deposited at 600ºC on CeO_2 overlying IBAD template.*

Task 3. Reducing defect density in epitaxial Ge on IBAD templates

We explored liquid phase processing techniques such as zone melting and recrystallization (ZMR) to reduce defect density in the epitaxial Ge on IBAD templates. A ZMR apparatus was set up using four halogen lamp heaters and several samples processed under different temperature, and vacuum conditions. Unfortunately, a problem we encountered was in vaporization of Ge at temperatures above 880°C, well below the melting point of Ge. So, while we tried to solve this problem, another approach that we investigated to reduce the defect density was to fabricate thicker eptiaxial Ge films on metal substrates. Ge films of four different thicknesses have been deposited by varying the tape speed from 2 cm/min to 0.25 cm/min. Details are shown in Table I.

Table I. *Thickness of epi Ge films on IBAD template*

Tape speed	Thickness (μm)
2 cm/min	0.73
1 cm/min	1.46
0.5 cm/min	2.92
0.25 cm/min	5.84

It was found that the in-plane texture became considerably sharp as Ge film thickness was increased as shown in Figure 8. As the figure shows, an in-plane texture as sharp as 1° FWHM was achieved in a 6 μm film indicating an average grain-to-grain misorientation as small as 1° over the entire sample.

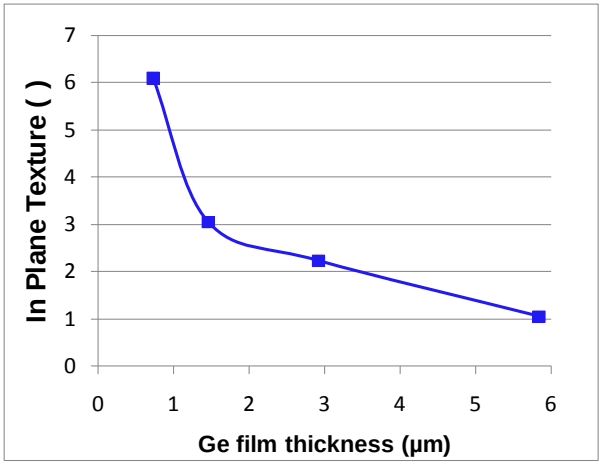

Figure 8 *Improvement in in-plane texture of Ge film grown on IBAD MgO template on metal substrate with increasing film thickness.*

Cross sectional TEM analysis was conducted on the 6 μm thick Ge film on metal substrate to evaluate how the defect density changed with film thickness and the results are shown in Figures 9, 10 and 11. Figure 9 displays the lower part of the film where an abundance of threading dislocations can be observed near the CeO_2 interface. A closer view of the various interfaces in the film in Figure 10 shows that several of the defects could have propagated even from MgO layer and through the $LaMnO_3$, CeO_2 and into the Ge layer. On a positive note, it seen in Figure 11, that the defect density is reduced significantly in the top part of the film.

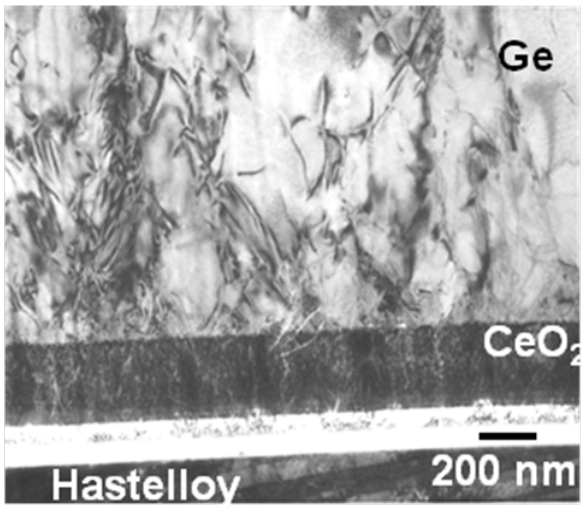

Figure 9 *Cross sectional TEM from Ge film grown on IBAD MgO template on metal substrate showing a high defect density near the Ge – CeO_2 interface.*

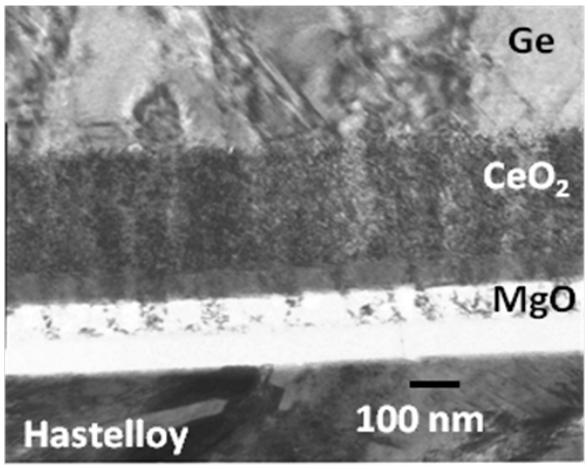

Figure 10 *Cross sectional TEM from Ge film grown on IBAD MgO template on metal substrate showing defects originating from MgO layer and propagating through all the epilayers.*

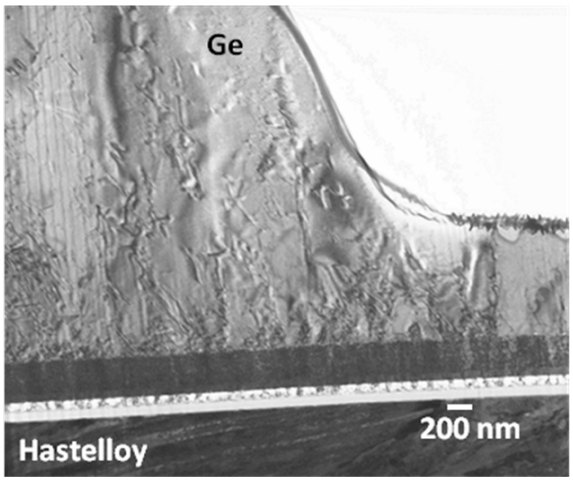

Figure 11 *Cross sectional TEM from 6 µm thick Ge film grown on IBAD MgO template on metal substrate showing reduction in defect density in the top part of the film.*

In order to quantify the dislocation density, high resolution XRD was performed on thicker samples i.e. 1.46, 2.92 and 5.84 µm thick samples. Figure 12 shows the width of the (001) peak improves with increasing thickness from 3900 to 3100 arc seconds.

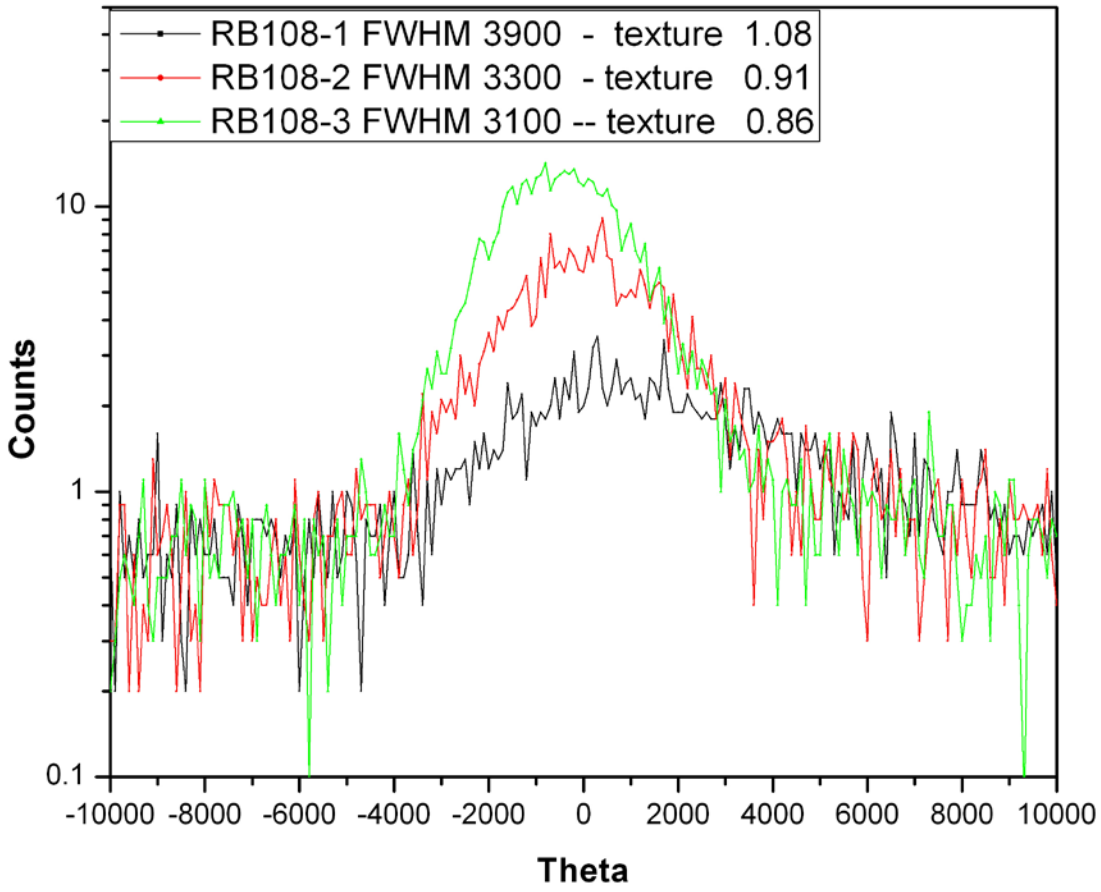

Figure 12 *High resolution XRD obtained thick Ge films grown on IBAD MgO template on flexible substrate*

Defect densities have been calculated from the peak widths from Figure 12 and are listed in Table II. A moderate reduction in defect density is observed but not significant compared to improvement in in-plane texture shown in Figure 1.

Table II. *Defect density in epitaxial Ge films on IBAD template flexible metal substrate*

Thickness (μm)	Defect density (#/cm^2)
1.46	5.1×10^8
2.92	3.7×10^8
5.84	3.3×10^8

Etch Pit density measurements:

In order to facilitate sample evaluation and optimization of the thin film deposition process, it is necessary to quantify the defect densities faster than with high resolution XRD measurements. So, we developed a procedure for defect density identification by etch pit density method. After conducting experiments with a various combinations of etchants, we concluded that etching in $KMnO_4$ and HF solution created etch pits with cleaner surface.

Etch pit experiments were conducted on the Ge film on epitaxial layers. Figures 13 and 14 show the microstructure of the top surface of epitaxial Ge films on IBAD templates before and after etching. The grain size of the Ge film is seen to be less than 200 nm. Etch pits are clearly obvious especially near the grain boundaries and their density is estimated to be about 5×10^8 cm^{-2}.

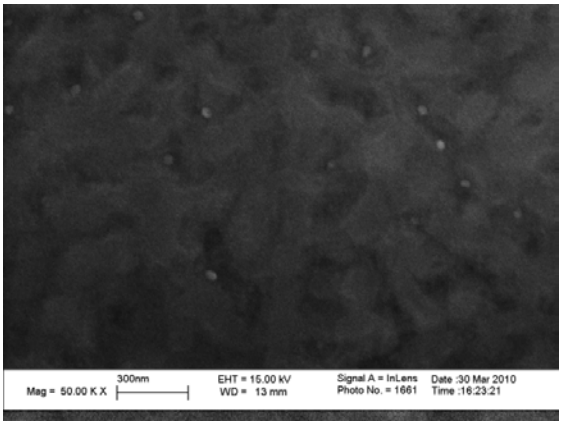

Figure 13 *Surface microstructure of an as-grown epitaxial Ge film on metal substrate*

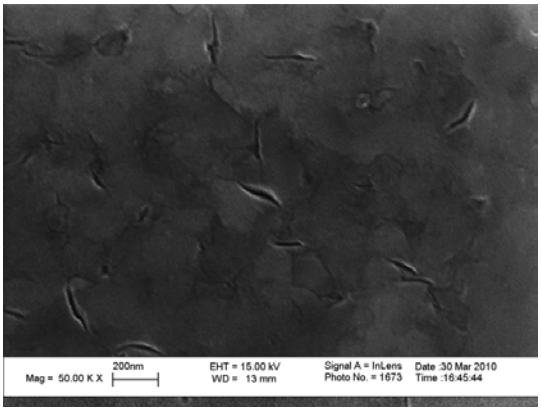

Figure 14 *Surface microstructure of an epitaxial Ge film on metal substrate after etch-pit experiment.*

Next, etch pit density measurements were conducted on samples of different Ge film thickness as described in Table I and the results are shown in Figure 15. The etch pitch density was found to decrease with increasing Ge film thickness which is in accordance with the results obtained from High resolution XRD. It is seen that the shape of the etch pits are square and elongated. Square-shaped pits are formed by the etching of the (004) planes with sides formed by the (111) planes. However, there is significant density of elongated pits formed mostly at the grain boundaries. It has been reported in the literature that elongated pit formation occurs while etching (110) planes. Etching of the few (220) oriented grains in our films could be responsible the elongated etch pits on a (001) surface.

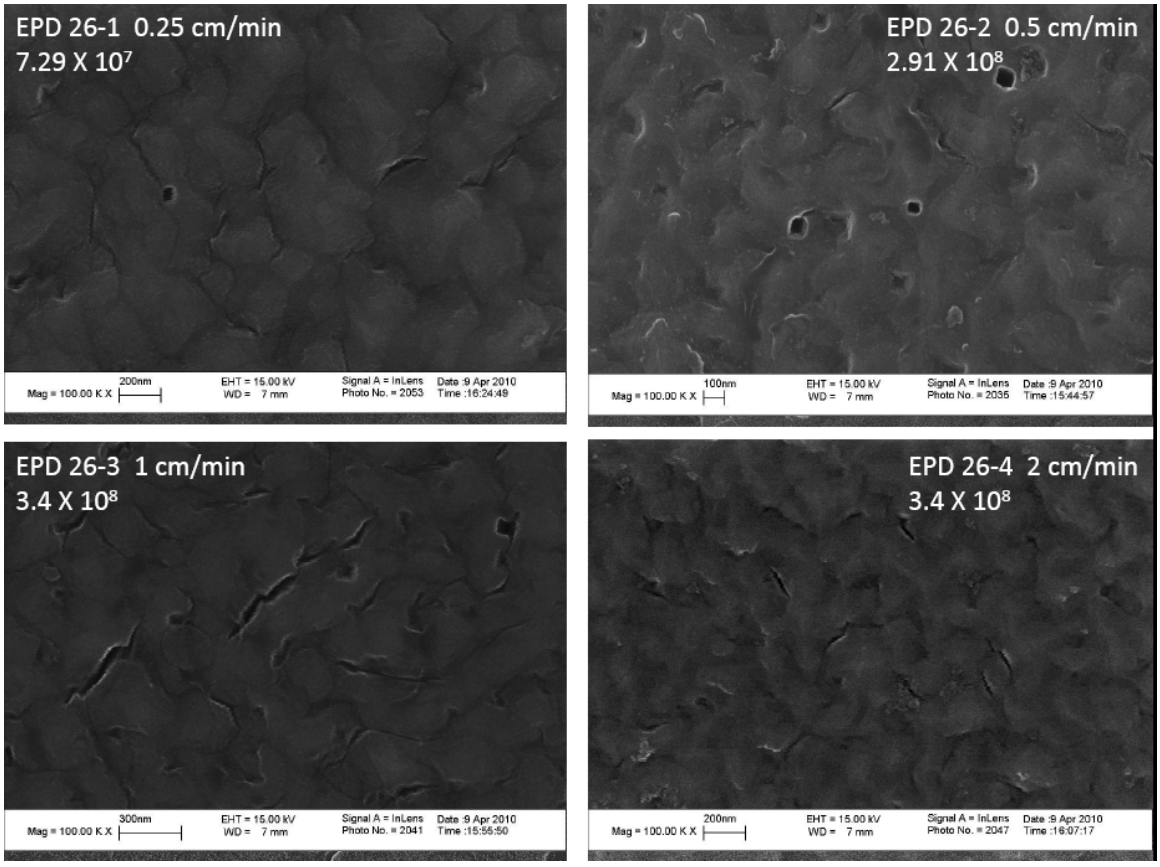

Figure 15 *Surface microstructures of epitaxial Ge films of different thickness on metal substrate after etch-pit experiment.*

Task 4 - Epitaxial Growth and Characterization of GaAs epilayers on IBAD coated flexible metal substrates

Here we report our progress in the development of MBE grown single crystalline GaAs epilayers on epitaxial Ge on IBAD-coated flexible polycrystalline metallic substrates. Samples (1cm x1.2 cm) were mounted In-free on Molybdenum blocks. Ge native oxide was thermally removed in vacuum and the Ge coated substrate was subsequently annealed at high temperatures (at 600<T<800°C) prior to introduction in MBE chamber. Upon introduction and for temperature exceeding 450°C the Ge surface showed a c(2x2) (mixed (2x1)(1x2)) reconstruction, typical of (001) Ge surface. In all attempts the GaAs growth was initiated at relatively low temperature (~400°C) and a thin (20nm) nucleation layer of GaAs was deposited, followed by an annealing step under As_2. Subsequently 1 micron-thick GaAs epilayers were deposited in standard growth conditions (growth rate ~ 1ML/sec T~550°C). The entire growth sequence was monitored by RHEED.

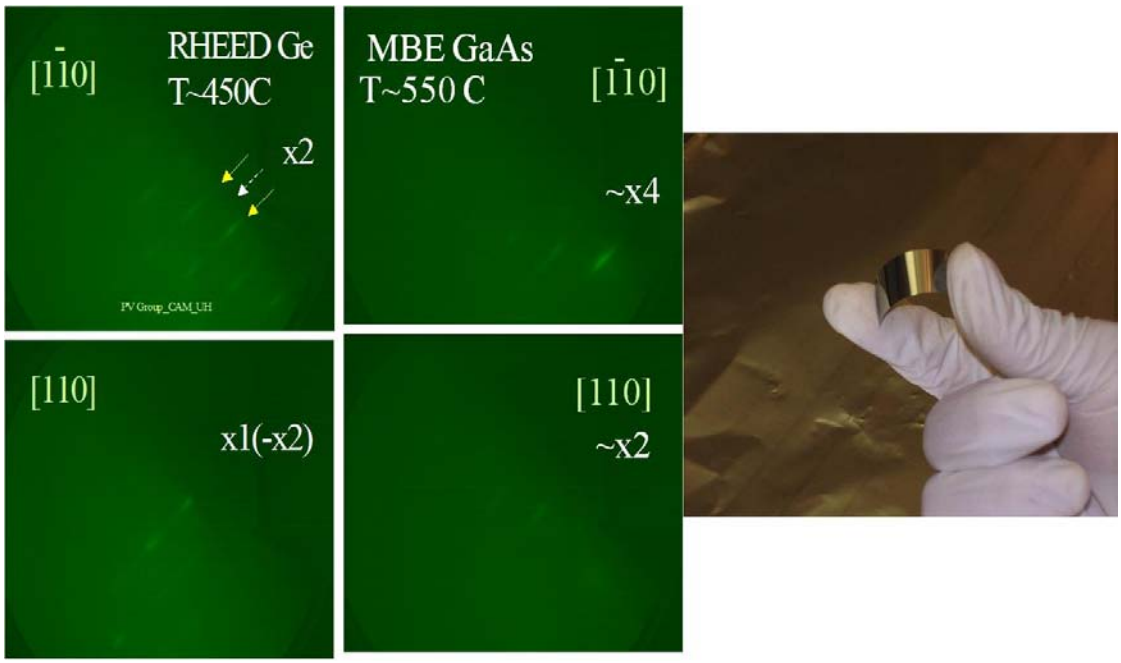

Figure 16 *(Left) RHEED of c(2x2) Ge coated flexible metal after oxide desorption and thermal annealing. (Middle) 2x4 RHEED diagram during the subsequent GaAs epilayer growth (Right) Photograph of fabricated flexible sample.*

The self -annihilation of anti-phase boundaries (mixed 2x4, 4x2 RHEED diagram), was observed for thicknesses exceeding ranging from 100-200 nm where a 2x4 RHEED diagram typical of a single domain (001) GaAs was recorded (Figure 16).

Epilayers exhibited a specular morphology. Also, flexibility was preserved after the epitaxial growth (Fig. 16). High resolution X-ray diffraction analysis confirmed the single crystalline (001) nature of GaAs (Figure 17). Cross-sectional transmission electron microscopy and full-width-at-half-maximum (FWHM) of the (004) diffraction peaks (~ 30 arcmin) obtained through high-resolution X-ray Diffraction (HR-XRD) suggested a defect density (dislocations) in the 10^8 cm^{-2} range.

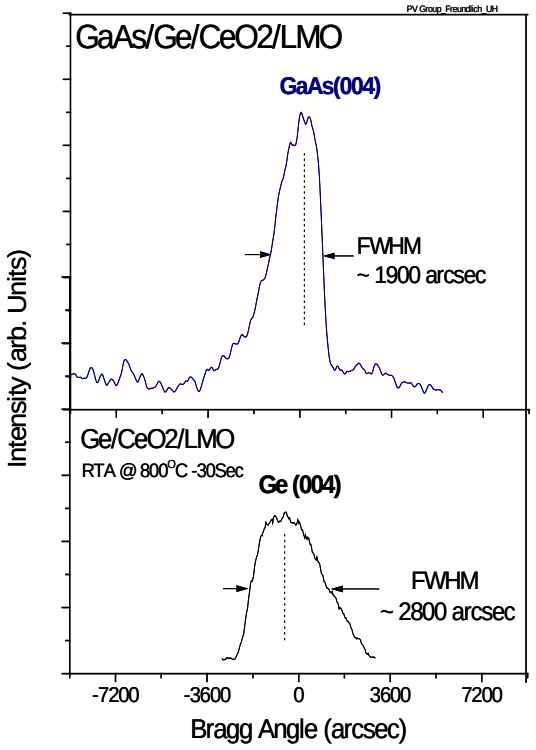

Figure 17. *HRXRD rocking curves recorded from IBAD coated Ge and after the MBE growth of GaAs.*

Temperature dependent photoluminescence (PL) analysis revealed a strong PL in as-grown samples (Figure 18). The low temperature photoluminescence was found to be dominated with DA –eA like bands in the 1.4-1.5 eV range and a relatively broad deeper luminescence band at 1.3 - 1.35 eV. At low temperature, the GaAs excitonic emission was detected at 1.526 eV (FWHM~20 meV) and was found to be slightly red shifted compared to the typical A_0X exciton in homoepitaxial GaAs. The magnitude of this red-shift (13 meV) suggested the absence of any significant thermoelastic/lattice mismatch strain (ε<0.1%) in the epilayers.

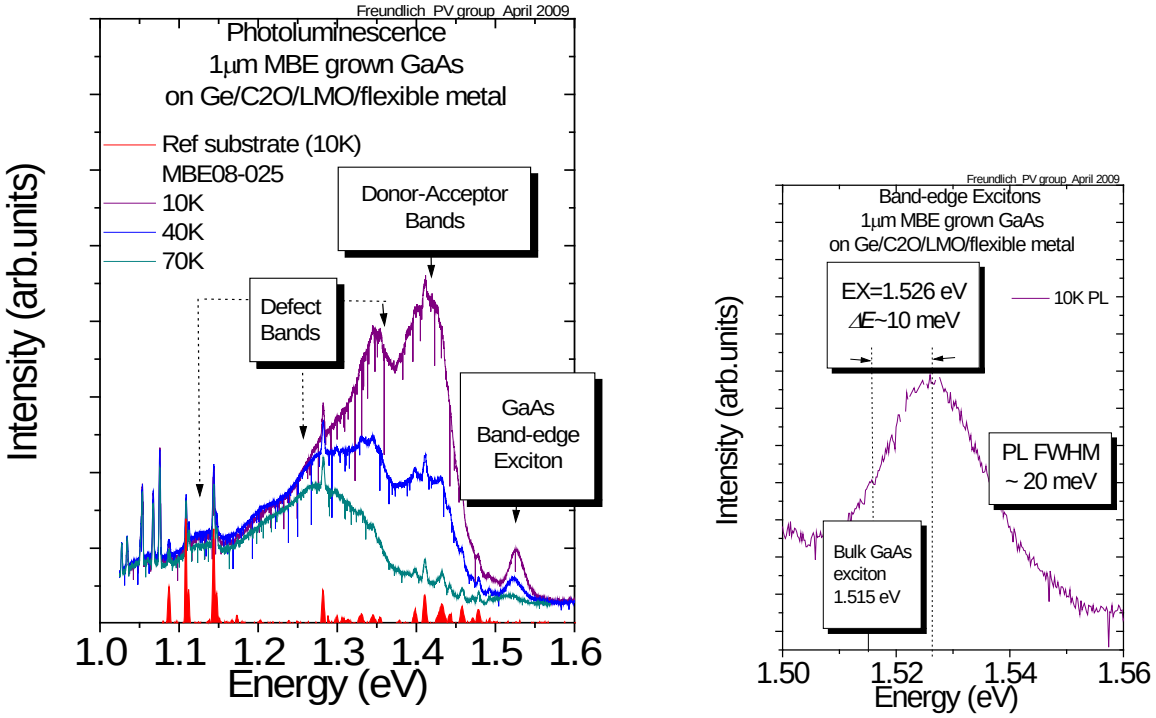

Figure 18. *Photoluminescence analysis MBE grown single crystalline GaAs on Ge coated flexible metal substrate (left) temperature dependent PL (right) zoomed near bandage excitonic region*

Assuming a conventional GaAs solar cell design and using established methodologies and accounting for defect densities extracted from TEM (~10^8 -$10^9$$cm^{-2}$) suggests that the present materials would only offer possibilities for the development of 5-10 % AM0 efficient single junction GaAs. While work on additional defect filtering and fabrication of improved GaAs photovoltaics is in progress, we have also evaluated modified device design that would support the development of high efficiency (>>10%) devices with current dislocation levels.

Modeling novel defect tolerant GaAs device designs

The modeling effort included the modification of the of the existing Matlab based source code for modeling of GaAs-based solar cells to include the reduction of the minority carrier lifetimes to simulate the operation of a solar cell made with defect bearing GaAs like that encountered currently with GaAs on flexible metal substrate

Modeling efficiency of a conventional GaAs solar cell

We present here the model of GaAs solar cell, with varying base and emitter thicknesses. The characteristics of the cell include absorption coefficient of GaAs, diffusions lengths and diffusion coefficient as a function of doping, $Al_xGa_{1-x}As$ window layer, Shockley-Read-Hall (SRH) recombination, from a single trap present at the midgap in depleted region. The n-type doping range is 10^{17} to $10^{18}cm^{-3}$ while the p-type doping range is between 10^{18} and $5*10^{18}cm^{-3}$, SRH lifetime is around 10^{-8} sec to $5*10^{-8}$ sec while the surface recombination velocity is in the order of 10^2 -10^3cm/sec due to the use of AlGaAs window layer (Fig. 19). Use of Anti reflective coating reduces the loss of light by reflection to 2% while other 5% is lost due to the shadowing effect of the grid contacts. Under AM0, this single junction GaAs solar cell, has optimized value of emitter and base thickness of around 0.7 and 1.7 microns respectively, to give us maximum efficiency of 24.2% (Fig. 20).

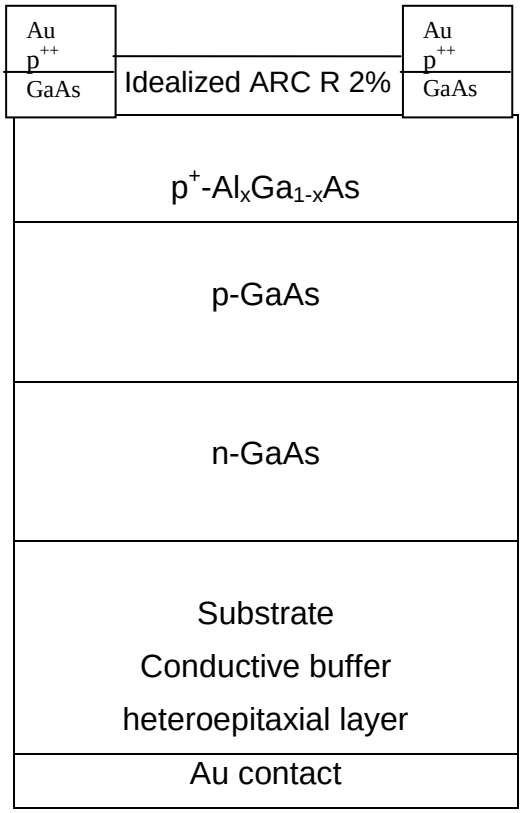

Figure 19 *Conventional GaAs solar cell device structure*

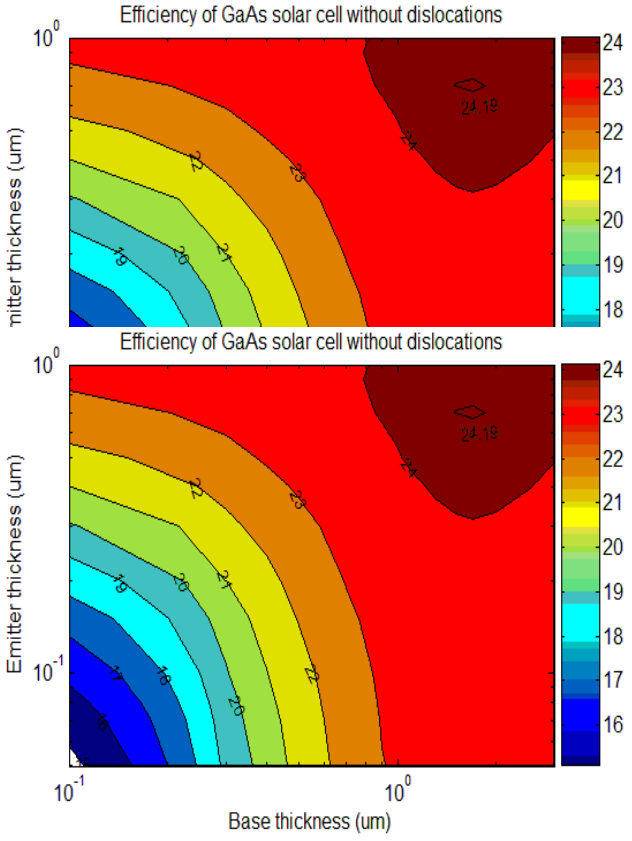

Figure 20 η *vs (Base/Emitter) thickness plot for conventional GaAs solar cell*

Modeling GaAs solar cells with dislocations

Dislocations are formed when there is lattice mismatch between epilayers (GaAs grown on Si substrate) or when iii-v semiconductors are grown on metallic flexible substrates. Dislocations play a dominant role in determining the properties of GaAs solar cells. The dislocations present in solar cell act as recombination center and reduce the lifetime and diffusion length of minority carriers according to relation,

$$\frac{1}{L^2} = \frac{1}{{L_0}^2} + \frac{N_{\mathrm{dis}}.\pi^3}{4} \qquad (1)$$

Where L is the net diffusion length, L_0 is the diffusion length of GaAs, N_{dis} is the dislocation density in the crystal. The reduction in diffusion length causes the current to decrease since minority carriers recombine before they can reach the surface. Hence by optimizing the device thickness, higher efficiencies can be achieved even for high dislocation densities. From efficiency vs thickness contour plot (Figure 21) it appears that despite a rather high dislocation densities of 10^8 cm^{-2} a device with optimized emitter and base design could deliver efficiency of 17.3% up nearly by 10 efficiency points from the 7.6% efficiency expected for conventional GaAs solar cell design.

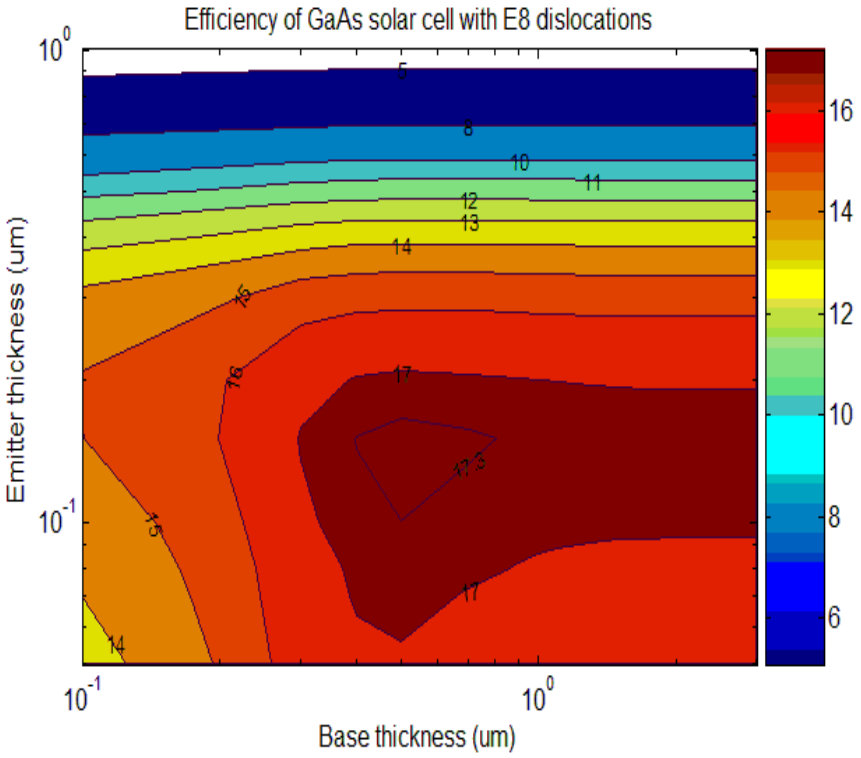

Figure 21 *Example of Efficiency (η) contour plot vs device "Base" and "Emitter" thickness contour plot for a device operating in the presence of a dislocation density in the range of 10^8 cm^{-2} dislocations.*

The calculation was then extended to different dislocation density ranges and for each defect density a set of optimal device thickness and doping was derived. Consequently the study allowed us to predict that at dislocation densities of 10^7, 10^8 and 10^9 cm^{-2} highly efficient cells can be fabricated. Results are summarized in Figure 22.

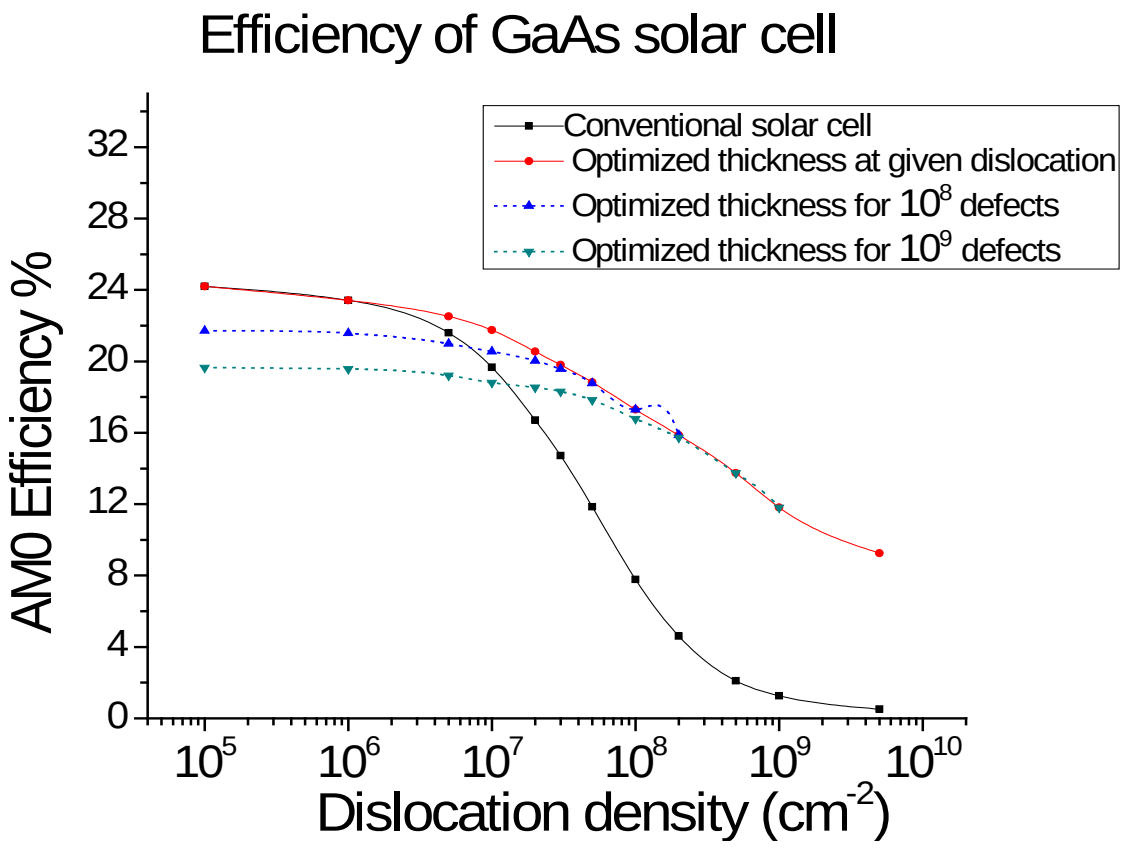

Figure 22. η *vs dislocation density plot for conventional design (black) and optimized design (red)*

In an attempt to further minimize/eliminate the formation of stacking faults and antiphase boundaries, we retrofitted our Molecular Beam Epitaxy (MBE) facilities with a Ge effusion cell and thin epitaxial layer of Ge was deposited prior to the initiation of GaAs growth. As illustrated in Figure 23, incorporation of the Ge bi-atomic step MBE buffer resulted in a two-fold reduction of the X-ray linewidth GaAs, suggesting an overall four-fold reduction in TDDs to about 10^8 cm^{-2} for a typical micron thick GaAs.

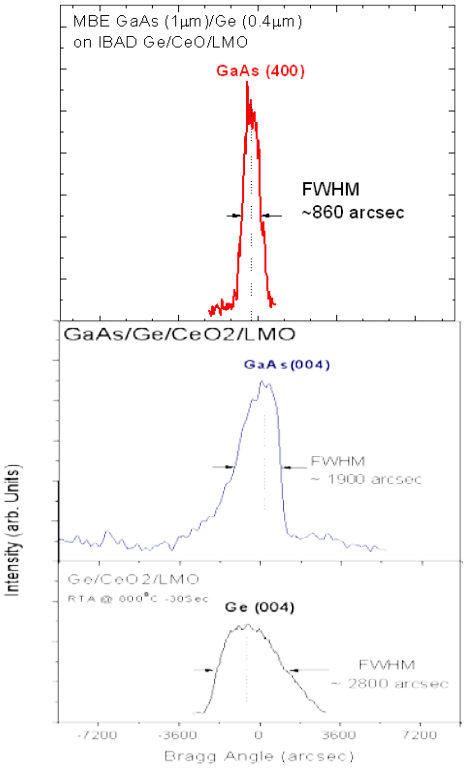

Figure 23. *High resolution (400) X-ray diffraction of (bottom) the initial Ge, (middle) a micron-thick GaAs grown directly on IBAD coated Ge, and (top) 1 μm thick GaAs deposited following MBE Ge deposition showing significant peak width (defect) reduction*

Task 5. Fabrication and testing of photovoltaic properties of GaAs solar cells deposited on IBAD templates on Hastelloy substrates

We also worked on fabricating complete GaAs solar cells using our existing Ge films. A simple non-intrusive photoresist based lithographic process has been recently optimized at UH, that allows in a single mesa etch and metal evaporation/resisit lift-off to define high quality patterns on GaAs coated flexible substrates. Patterns resolution of few microns with well-defined grid line of 30 microns have been realized on few cm square flexible templates (Figure 24). Furthermore, the approach seems scalable to much wider substrate widths and length.

Two solar cells were fabricated using the architecture discussed previously. Unfortunately, they were found to be shorted. TEM analysis shows presence of Ge in the GaAs layer, presence of substrate species in the Ge layer as well as an undulating top contact layer. Any or all of these could have contributed to the short. We are

working on addressing these issues and will evaluate the benefit of our demonstration of epitaxial III-V solar cells on inexpensive substrates.

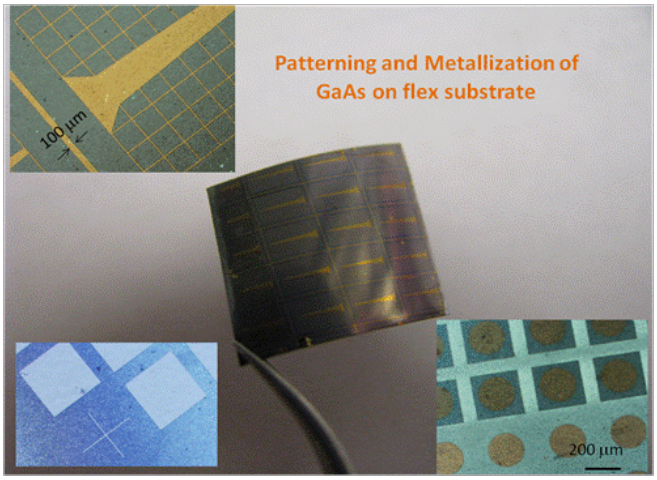

Figure 24. *Photograph of 12x12 mm patterned device structure on flexible substrate (top left) micrograph showing the top grid on GaAs mesa (bottom right) micrograph of TLM/diode patterns with deep mesa showing excellent edge resolution (bottom left) micrograph of mesa etch resolution (cross width 10 µm).*

Patents: None

Publications/Presentations/Travel:

1. "Virtual" single-crystalline GaAs photovoltaics on flexible metal substrates" (Paper 7597-7) 16th Symposium on Physics and Simulation of Optoelectronic Devices, SPIE Photonic West, San Francisco CL, Jan 25, 2010.
2. "Novel, single-crystalline-like templates on low-cost, flexible substrates for high efficiency photovoltaics". Presented at the 35th Photovoltaics Specialist Conference, Honolulu, HI, June 21 – 25, 2010. Paper submitted to the proceedings of the conference.
3. "Single crystalline GaAs Photovoltaics on flexible metal substrates". Presented at the 35th Photovoltaics Specialist Conference, Honolulu, HI, June 21 – 25, 2010. Paper submitted to the proceedings of the conference.